Biophysical Journal Volume 96 January 2009 77–85

Membrane Transport of Singlet Oxygen Monitored by Dipole Potential Measurements

Valerij S. Sokolov[†] and Peter Pohl[‡§*]
[†]A. N Frumkin Institute of Physical Chemistry and Electrochemistry, Russian Academy of Science, Moscow, Russia;
[‡]Institut für Biophysik, Johannes Kepler Universität Linz, Austria; and [§]Leibniz Institut für Molekulare Pharmakologie, Berlin, Germany

ABSTRACT The efficiency of photodynamic reactions depends on 1), the penetration depth of the photosensitizer into the membrane and 2), the sidedness of the target. Molecules which are susceptible to singlet oxygen ($^1O_2$) experience less damage when separated from the photosensitizer by the membrane. Since $^1O_2$ lifetime in the membrane environment is orders of magnitude longer than the time required for nonexcited oxygen (O_2) to cross the membrane, this observation suggests that differences between the permeabilities or membrane partition of $^1O_2$ and O_2 exist. We investigated this hypothesis by releasing $^1O_2$ at one side of a planar membrane while monitoring the kinetics of target damage at the opposite side of the same membrane. Damage to the target, represented by dipole-modifying molecules (phloretin or phlorizin), was indicated by changes in the interleaflet dipole potential difference $\Delta\varphi_b$. A simple analytical model allowed estimation of the $^1O_2$ interleaflet concentration difference from the rate at which $\Delta\varphi_b$ changed. It confirmed that the lower limit of $^1O_2$ permeability is ~2 cm/s; i.e., it roughly matches O_2 permeability as predicted by Overton's rule. Consequently, the membrane cannot act as a barrier to $^1O_2$ diffusion. Differences in the reaction rates at the cytoplasmic and extracellular membrane leaflets may be attributed only to $^1O_2$ quenchers inside the membrane.

INTRODUCTION

Photodynamic therapy explores photosensitizers' ability to accumulate selectively within tumor cells and kill these cells upon illumination by visible light (compare Levy (1)). Cell death is caused by a reactive oxygen species such as singlet oxygen ($^1O_2$), which is generated by excited photosensitizer molecules. If photosensitizers are bound to the cell membrane or entrapped in endocytic vesicles, the effectiveness of damage exerted by $^1O_2$ must depend on membrane permeability to $^1O_2$ (P_{1O}). Although crucial for the understanding of photodynamic reactions on the molecular level, no successful direct measurements of P_{1O} have yet been reported to our knowledge.

As for any other molecule, membrane permeability of $^1O_2$ can be calculated if the concentration ($[^1O_2]$) and the mobility (D_{1O}) within the membrane are known. For triplet oxygen (O_2), the product of both parameters $D_O[O_2]$ has been determined by electron spin resonance (ESR). It is equal to or twice the corresponding bulk value in water if measured close to the membrane-water interface or in the middle of the membrane, respectively (2–4). The ratio may increase to a value of five in the membrane center, depending on membrane composition and temperature. Hence, O_2 membrane permeability (P_O) was estimated to vary between 42 and 230 cm/s (4,5).

In analogy to P_O, P_{1O} is also expected to depend on membrane composition. Measurements of P_{1O}, however, are fraught with additional difficulties caused by the limited lifetime of $^1O_2$. It varies between 13 and 35 μs in lipid bilayers (6) depending on membrane composition. If P_{1O} was equal to P_O, such a lifespan would be sufficient to cross the membrane thousands of times. Consequently, the difference in concentrations between $^1O_2$ molecules released at the outer leaflet of a plasma membrane and those molecules that reach the inner leaflet should be negligibly small. However, contrasting experimental results were obtained (7,8). For example, we found that the photodynamic reaction may take place in one leaflet only; i.e., the amount of target molecules damaged in the leaflet facing the photosensitizer was roughly identical to the total amount of target molecules inactivated. This result suggested that only a limited amount of the reactive oxygen species diffuses across the membrane (9). A possible explanation would be that the highly abundant target molecules trapped most of the reactive oxygen species. This reasoning is in line with reports according to which efficient $^1O_2$ membrane traps prevent up to 90% of $^1O_2$ from being released from the membrane (7,8).

Consequently, investigation of P_{1O} requires the membrane to be free of $^1O_2$ traps. The target molecule has to be exclusively located at one membrane-water interface while $^1O_2$ is released at the opposite interface. In this study, phloretin and phlorizin played the above-mentioned role of target molecules (Fig. 1). These substances are known as natural antioxidants—scavengers of reactive oxygen species belonging to the wide class of flavonoids (10). These substances are also known to change the dipole potential drop at the membrane-water interface upon adsorption to the membrane (11–14). The interleaflet difference in the potential drop ($\Delta\varphi_b$) is, thus, a convenient measure for the interleaflet asymmetry

Submitted April 10, 2008, and accepted for publication September 3, 2008.

*Correspondence: peter.pohl@jku.at

Editor: Francisco Bezanilla.

0006-3495/09/01/0077/9 $2.00

doi: 10.1529/biophysj.108.135145

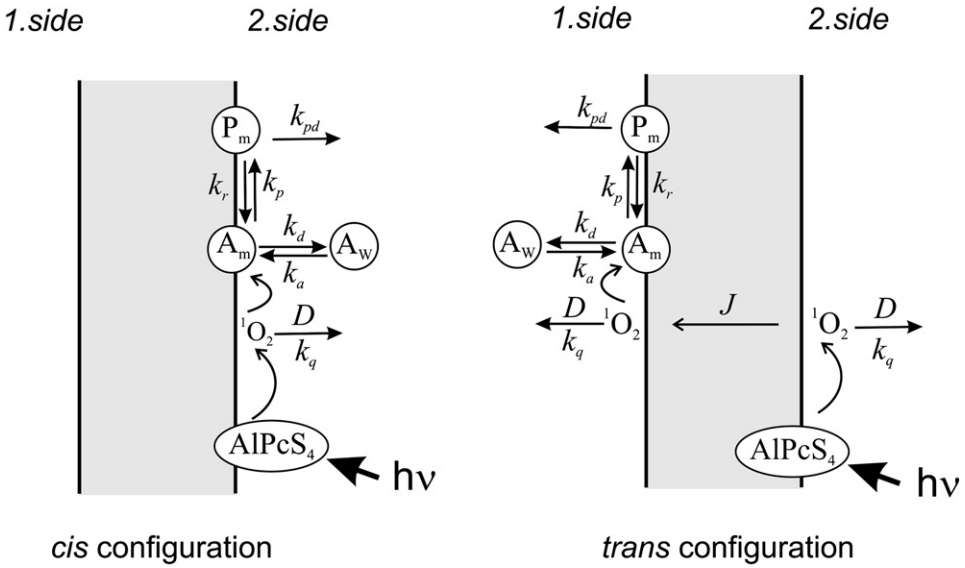

FIGURE 1 Scheme of the experimental arrangement in *cis* and *trans* configurations. Singlet oxygen ($^1O_2$) is produced by the photosensitizer ($AlPcS_4$) upon illumination with light of a wavelength of 670 nm. Target (phlorizin) adsorption and desorption occurs with the rate constants k_a and k_d, respectively. The photoproduct desorbs with k_{pd}. D and k_q are the aqueous diffusion coefficient of singlet oxygen ($^1O_2$) and the rate constant of $^1O_2$ quenching in aqueous solutions, respectively. P_m, A_m, and A_w, denote membrane product, membrane target, and aqueous target concentrations, respectively. The rate constants of the forward and reverse reactions are indicated as k_p and k_r, respectively.

of target destruction. We used $\Delta\varphi_b$ to estimate the transmembrane $^1O_2$ concentration difference and, thus, to assess P_{1O}.

MATERIALS AND METHODS

Black planar lipid membranes were formed using a traditional method (15) in the orifice of a Teflon septum which separated two aqueous solutions. They were made of a 1.5% L-α-diphytanoyl-lecithin (Avanti Polar Lipids, Alabaster, AL) solution in *n*-decane (Merck, Darmstadt, Germany). This lipid was chosen because it does not contain double bonds and is, therefore, not labile to oxidation by $^1O_2$. As a consequence, membranes formed from such lipids are stable even when $^1O_2$ is released by membrane-bound photosensitizer (16,17).

The aqueous compartments at both sides of the membrane were continuously stirred by magnetic beads. They contained KCl (Merck), 3-cyclohexilamino-2-hydroxy-1-propanesulphonic acid (CAPSO, Fluka, St. Gallen, Switzerland), morpholinethane sulphonic acid (MES, Boehringer, Mannheim, Germany), NaH_2PO_4 (Merck), imidazole (Serva, Heidelberg, Germany), and HEPES (Sigma, Deisenhofen, Germany), which were dissolved in twice-distilled water.

A high power mercury-xenon lamp (1 kW) illuminated the planar bilayer through an optically transparent window of the first compartment (9,18). After the illuminating light passed both an aqueous filter and a monochromator (Oriel Instruments, Stratford, CT) set at a wavelength of 670 nm (band pass 20–40 nm), it was focused onto the membrane. In the focus, a thermoelement (RTN-31C, VNIIOFI, Moscow, Russia) measured light intensity of ~20 W/m^2. Light intensity was varied with the aid of neutral glass filters (Edmund Scientific, Barrington, NJ).

Aluminum phthalocyanine tetrasulfonate ($AlPcS_4$, Porphyrine Products, Logan, UT) generates $^1O_2$ upon illumination. $AlPcS_4$ was added from an aqueous stock solution to the second side of the membrane. Phloretin or phlorizin (Sigma) were added from an ethanolic stock solution either into the same (second) compartment or into the first compartment. The total ethanol concentration in the aqueous compartments never exceeded 1%. Sodium azide (Sigma) was added to the aqueous solutions on both sides of the membrane. Coenzyme Q2 (Sigma) was dissolved in the membrane-forming solution.

Membrane capacitance and conductance were continuously measured. Therefore, a triangle alternating input voltage was passed through a silver/silver chloride electrode and a connecting agar bridge to the second side of the membrane. The output signal was transferred via a reference electrode at the first side of the membrane to a current-voltage converter (model 428, Keithley Instruments, Cleveland, OH). It maintained the electric potential of the electrode in the first compartment at virtual zero with respect to ground. The amplified signal was visualized and stored by a digital oscilloscope (model TDS-340, Tektronix, Wilsonville, OR). It was equipped with a general purpose interface bus (GPIB) allowing data transfer to a personal computer and subsequent calculation of membrane capacitance and conductance.

$\Delta\varphi_b$ was measured by the intramembrane field compensation method using the second harmonic of the capacitive current (19, see also reviews 20,21). The method exploits the nonmonotonic voltage dependence of membrane capacitance (22). Membrane capacitance is minimal if both the voltage between the aqueous solutions is zero and the interfacial membrane potentials (i.e., the sum of membrane surface and dipole potentials) at the first and second sides are equal to each other. As membrane adsorption of a charged or dipolar molecule to one of the leaflets gives rise to $\Delta\varphi_b \neq 0$, membrane capacitance increases. It returns to its minimum if the voltage between the aqueous solutions is also changed, such that the electric field between the two aqueous membrane interfaces is counterbalanced; i.e., if the absolute value of this voltage is equal to $\Delta\varphi_b$. The voltage corresponding to the minimum of capacitance was found as the direct current (DC) bias of the sine voltage applied by a digital lock-in amplifier (model 7265, Ametek, Oak Ridge, TN) to the second side of the membrane, at which a second harmonic of capacitive current vanished. The electrode at the first side was connected with the input of a current-voltage converter (model 428, Keithley Instruments). If referring to the conventional nomenclature of cell experiments, the polarity of $\Delta\varphi_b$ would be equal to that of cell membrane potential if the first compartment was extracellular and the second one was intracellular.

The second harmonic of the output voltage was measured by the lock-in amplifier, which transmitted its value via GPIB interface to a computer. A self-made software routine provided negative feedback which maintained zero level of second harmonics by adjusting the DC voltage bias every 0.5 s. As this DC voltage is equal to $\Delta\varphi_b$, it was recorded as a function of time and stored in the computer. If the experiment was repeated at least five times, the standard error of $\Delta\varphi_b$ is indicated. Otherwise only the mean value of $\Delta\varphi_b$ is given.

RESULTS

Addition of phloretin or phlorizin into one of the aqueous compartments changed $\Delta\varphi_b$ due to the adsorption of their oriented dipoles to the adjacent leaflet. $\Delta\varphi_b$ depended on the aqueous concentration of these compounds, as has been previously observed (13,14). Illumination did not affect $\Delta\varphi_b$ (not shown).

$AlPcS_4$ addition to the second compartment also generated a change in $\Delta\varphi_b$. Its sign indicated the adsorption of negatively charged molecules. $\Delta\varphi_b$ was very close to the ζ-potential measured when $AlPcS_4$ was allowed to adsorb to liposomes under similar conditions (18). $\Delta\varphi_b$ depended on the aqueous $AlPcS_4$ concentration and on the total ionic strength of the solution, i.e., the KCl concentration (Fig. 2). Again, illumination did not affect $\Delta\varphi_b$. Although illumination resulted in an excited state of $AlPcS_4$ and $^1O_2$ was released, there was no oxidative reaction in the absence of the target.

In contrast, if $AlPcS_4$ and one of the targets, i.e., one of the dipole modifiers (phloretin or phlorizin), were present, illumination altered $\Delta\varphi_b$ (Fig. 3). The experiments were carried out in *cis* and *trans* configurations. Addition of both the target and $AlPcS_4$ into the second compartment was denoted *cis* configuration (Fig. 3 *A*), and target addition into the first compartment (while $AlPcS_4$ was still added to the second compartment) was called *trans* configuration (Fig. 3 *B*). Accordingly, phlorizin increased $\Delta\varphi_b$ in the *cis* configuration and decreased $\Delta\varphi_b$ in the *trans* configuration. Illumination always acted in decreasing the absolute value of $\Delta\varphi_b$, suggesting that phloretin or phlorizin were damaged. The same conclusion was drawn from the observation that the photoeffect was proportional to the change in $\Delta\varphi_b$ introduced by phloretin or phlorizin adsorption (compare Fig. S1 in the Supplementary Material).

If the photoeffect was mediated by phloretin or phlorizin damage, $\Delta\varphi_b$ should be restored in the dark due to membrane adsorption of unmodified molecules from the bulk solutions. As expected, full recovery was observed in the *trans* configuration (Fig. 3). However, recovery was always incomplete in the *cis* configuration. The residual change in $\Delta\varphi_b$ indicated that hydrophobic products of the reaction between $^1O_2$ and phlorizin or phloretin also contributed to $\Delta\varphi_b$. As different product concentrations in the *cis* and *trans* arrangements reflect differences in the respective reaction rates (compare Sokolov et al. (9)), differences in the recovery levels were expected. Phloretin and phlorizin produced qualitatively similar results. We will focus mainly on the experiments with the membrane-impermeable (13) phlorizin, because it does not quench $^1O_2$ within the membrane.

To arrive at a quantitative description of the photoeffect, we used the sum of two exponential terms which satisfactorily approximated the dependence of $\Delta\varphi_b$ on illumination

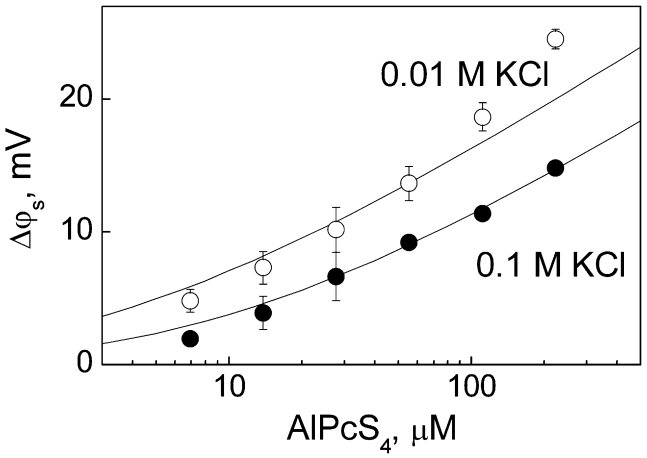

FIGURE 2 Dependence of membrane boundary potential ($\Delta\varphi_b$) on aqueous $AlPcS_4$ concentration. The buffer solution contained 100 mM KCl, 10 mM HEPES, pH 7.5 (*filled circles*) or 10 mM KCl, 1 mM HEPES, pH 7.5 (*open circles*). The lines represent the numerical solutions of adsorption $\sigma = zKC_a e^{-zF\phi_b/RT}$ and Gouy-Chapman $\sigma/\sqrt{8\varepsilon\varepsilon_0 RTc_1} = sh(F\phi_s/2RT)$ equations, where c_1, C_a, ε, ε_0, R, and T are, respectively, the aqueous KCl and $AlPcS_4$ concentrations, the dielectric permittivities of the aqueous solution and of vacuum, the gas constant, and the absolute temperature (299 K). Adsorption of $AlPcS_4$ anions with valence $z = 4$ to the initially uncharged lipid bilayer gives rise to the surface charge σ. σ, in turn, results in the experimentally determined membrane surface potential, φ_s. K relates the aqueous $AlPcS_4$ concentration to its membrane surface concentration. Its value of 200 C cm mol^{-1} was found as a fit parameter by minimizing the sum of square deviations. The standard error from at least five experiments is indicated by error bars.

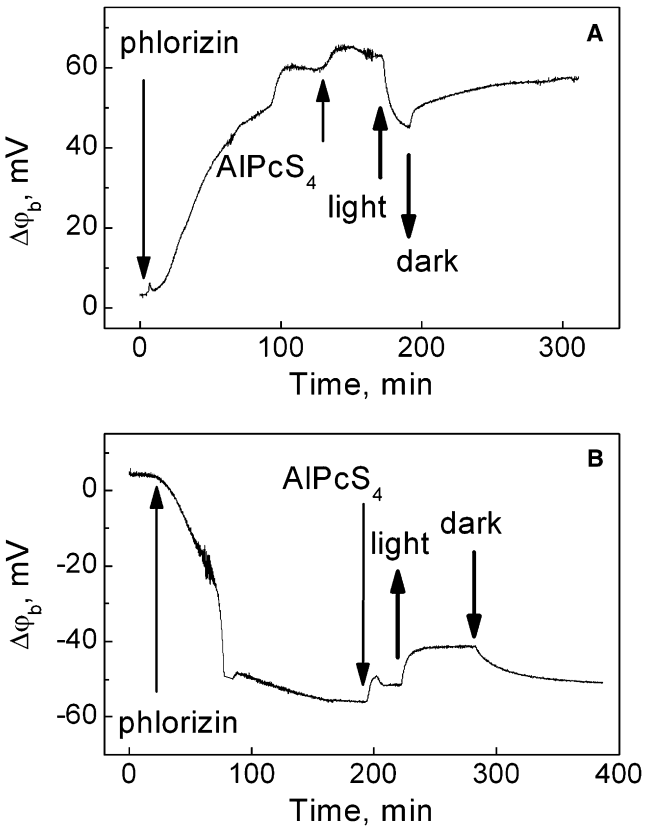

FIGURE 3 Typical kinetics of $\Delta\varphi_b$ changes during phlorizin and $AlPcS_4$ adsorption as well as during illumination. The experiment is shown in *cis* and *trans* configurations, when phlorizin and $AlPcS_4$ were on the same side of the membrane (*A*) and on opposite sides (*B*), respectively. Additions of phlorizin and $AlPcS_4$, as well as the illumination period, are marked with arrows. The buffer solution contained 100 mM KCl and 10 mM HEPES, pH 7.5.

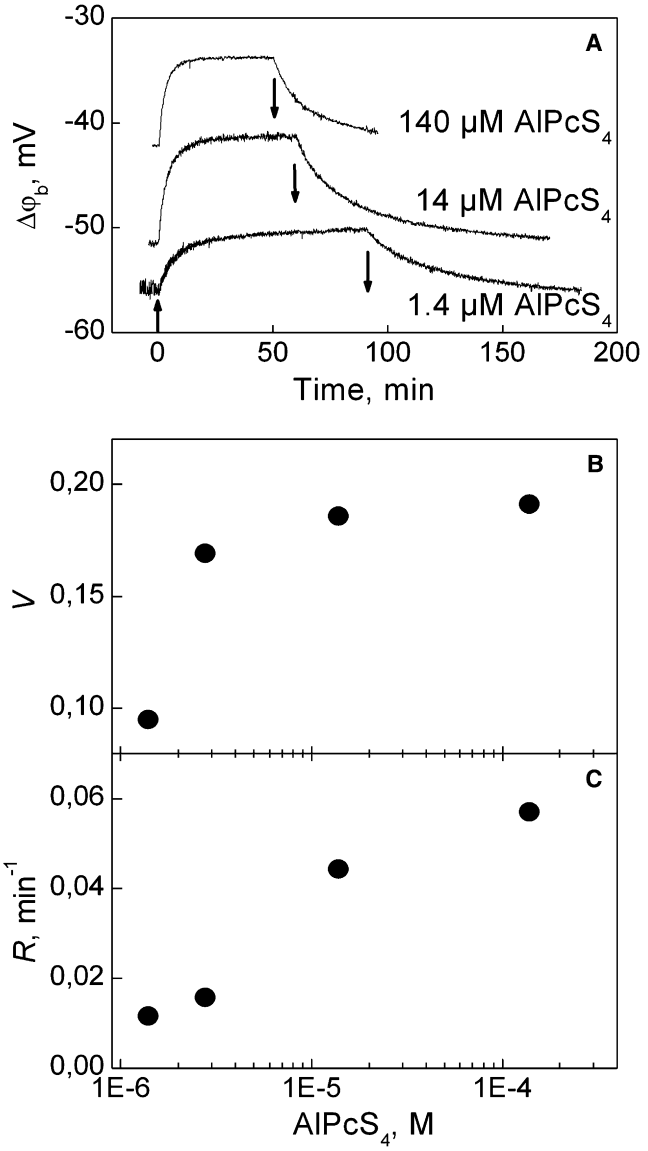

FIGURE 4 Effect of $AlPcS_4$ concentration on the photoeffect. Representative experimental records (*trans* configuration) of $\Delta\varphi_b$ are shown. The upturned and downturned arrows indicate beginning and end of illumination (*A*). The relative amplitude of the photoeffect (*V*) saturates with increasing $AlPcS_4$ concentration (*B*). In contrast, the initial rate *R* of the photoeffect is a linear function of $AlPcS_4$ concentration (*C*). For experimental conditions, see Fig. 3. The data points were averaged over at least three measurements.

time, *t*. We introduced the initial rate (*R*) and the final magnitude (*V*) as important parameters which are sufficient to describe the photoeffect (see Appendix A):

$$R = \left.\frac{\frac{d\varphi_b}{dt}}{\Delta\varphi_b}\right|_{t=0}; \; V = \frac{\Delta\varphi_b|_{t=0} - \Delta\varphi_b|_{t\to\infty}}{\Delta\varphi_b|_{t=0}}.$$

When the photoeffect was too slow to reach a steady state, *V* was determined as the limit of the two-exponential kinetics for $t \to \infty$.

Both *V* and *R* were augmented by releasing more $^1O_2$ per unit time. Experimentally, there are two possibilities: 1), the increase of the $AlPcS_4$ concentration and 2), the increase of light intensity, *I*. *V* saturated with increasing *I* and increasing membrane abundance of $AlPcS_4$ (Figs. 4 and 5). The experiment revealed that *V* was always smaller than 1, confirming thereby one of the above predictions: that $\Delta\varphi_b$ generated by the target molecules never vanishes. In contrast to *V*, *R* showed a linear dependence on $AlPcS_4$ abundance and *I* (Figs. 4 and 5). This observation justified the use of *R* as a measure of the photodynamic reaction rate. As predicted in the preceding paragraph, *R* was considerably higher in the *cis* configuration than in the *trans* configuration. $\Delta\varphi_b$ recovered with the same kinetics at all $AlPcS_4$ concentrations, the characteristic recovery time being close to the characteristic time of phlorizin adsorption (Figs. 3 and 4 *A*).

Since the adsorption of both phlorizin and $AlPcS_4$ (and thus $\Delta\varphi_b$) depended on pH, *R* and *V* were expected to depend on pH as well. In line with these anticipations, both *R* and *V* increased with increasing pH, up to pH 8 and 8.5, respectively (Fig. 6). Intriguingly, the maximum of the photoeffect was not observed in a pH range where $\Delta\varphi_b$ was maximal but at basic pH values, where $\Delta\varphi_b$ decreased with increasing pH. The result can be interpreted in terms of a photodynamic

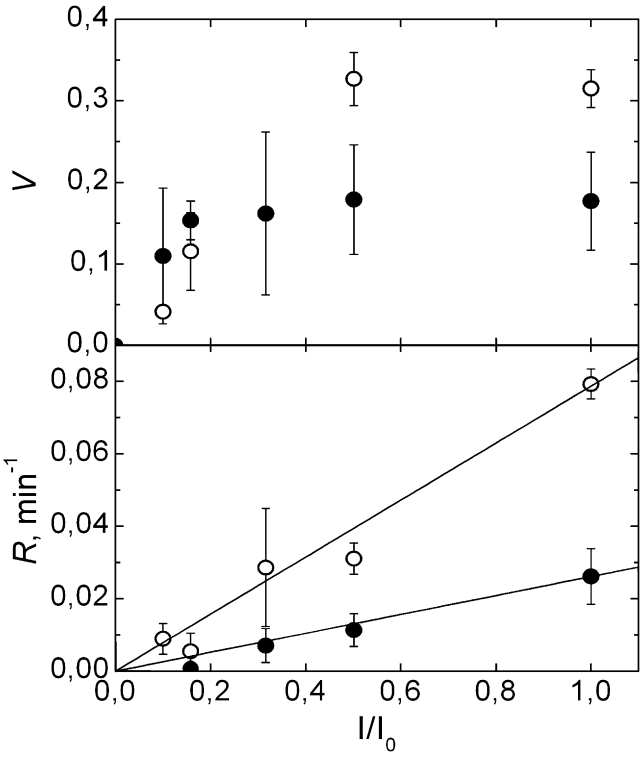

FIGURE 5 Dependence of amplitude *V* (*top*) and rate *R* (*bottom*) of the photoeffect on light intensity (*I*). Filled and open circles denote the experiments in *trans* and *cis* configurations, respectively. $AlPcS_4$ concentration was equal to 14 μM. All other conditions were as in Fig. 3. Linear regression (least-squares approximation) revealed slopes equal to 0.078 min^{-1} (*cis* configuration) and 0.026 min^{-1} (*trans* configuration).

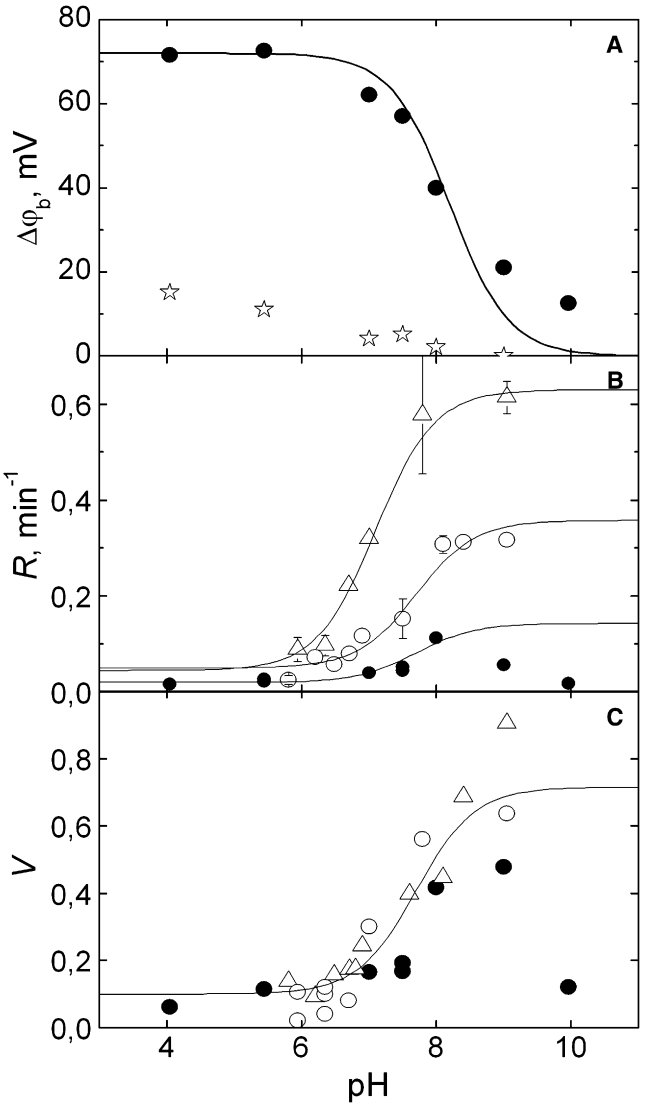

FIGURE 6 Effect of pH on the photoreaction. pH affects membrane adsorption of both phlorizin (50 μM, *squares*) and phthalocyanine (14 μM, *stars*). The solid line was calculated according to Eqs. 12A–13A with $\mu_A/\varepsilon\varepsilon_0 A_m = 72$ mV and $pK_A = 8.2$. (*A*). *V* (*B*) and *R* (*C*) also depended on pH. Open and solid symbols denote *cis* and *trans* configurations, respectively. The circles represent data obtained with phlorizin (50 μM), the triangles with phloretin (10 μM). $AlPcS_4$ concentration was 14 μM. The aqueous solution contained 0.1 M KCl and 1 mM buffer. Depending on bulk pH, we adopted buffer composition: KH_2PO_4 ($5 < pH < 6$), MES ($6 < pH < 7$), HEPES ($7 < pH < 8$), Tris ($8 < pH < 9$), and CAPSO ($9 < pH < 10$). The theoretical curves were plotted according to Eq. 2 using the following parameters: $k_p{}^1O_2 = 0.9$ min^{-1}, $\mu_P/\mu_A = 0.95$, $pK_A = 7.7$, $pK_P = 7.1$ (*triangles*); $k_p{}^1O_2 = 0.5$ min^{-1}, $\mu_P/\mu_A = 0.9$, $pK_A = 8.2$, $pK_P = 7.7$ (*solid circles*), $k_p{}^1O_2 = 0.2$ min^{-1}, $\mu_P/\mu_A = 0.9$, $pK_A = 8.2$, $pK_P = 7.7$ (*open circles*) (*B*); $k_d\mu_P/k_{pd}\mu_A = 0.9$, $pK_A = 8.2$, $pK_P = 7.7$ (*C*).

transformation of phlorizin into a product which 1), is a weak acid like the reactant; 2), has almost the same dipole moment; but 3), a 0.5 unit lower pK_a, and 4), adsorbs to the membrane only if uncharged (like phlorizin). Further increase in pH resulted in a decrease of the photoeffect because the amount of membrane-bound $AlPcS_4$ decreased, as indicated by the decline of $AlPcS_4$-mediated $\Delta\varphi_b$ (Fig. 6).

Since the acid base equilibrium is unlikely to be affected by the removal of the glucose moiety, the aglycon of phlorizin—phloretin—should exhibit the same pH dependence as phlorizin itself, which was confirmed experimentally. The slower kinetics in the presence of phlorizin may be due to its more superficial localization in the membrane or due to a protecting effect of the glucose moiety. The hypothesis that phloretin interacts more effectively with $^1O_2$ than phlorizin is in line with its ability to quench reactive oxygen species more effectively than phlorizin (10).

The photoeffect occurs at different rates in *cis* and *trans* configurations. Since neither phlorizin (13) nor the fourfold charged $AlPcS_4$ are able to penetrate the membrane (23), the *trans* effect can only be explained by assuming that $^1O_2$ permeates the membrane after having been released by the excited $AlPcS_4$. We have proven the involvement of $^1O_2$ in the *trans* effect by adding sodium azide. It quenched $^1O_2$. Consequently, *R* decreased (Fig. 7 *A*). Involvement of $^1O_2$ in the photoreaction was confirmed by yet another quencher of singlet oxygen: the lipid-soluble coenzyme Q

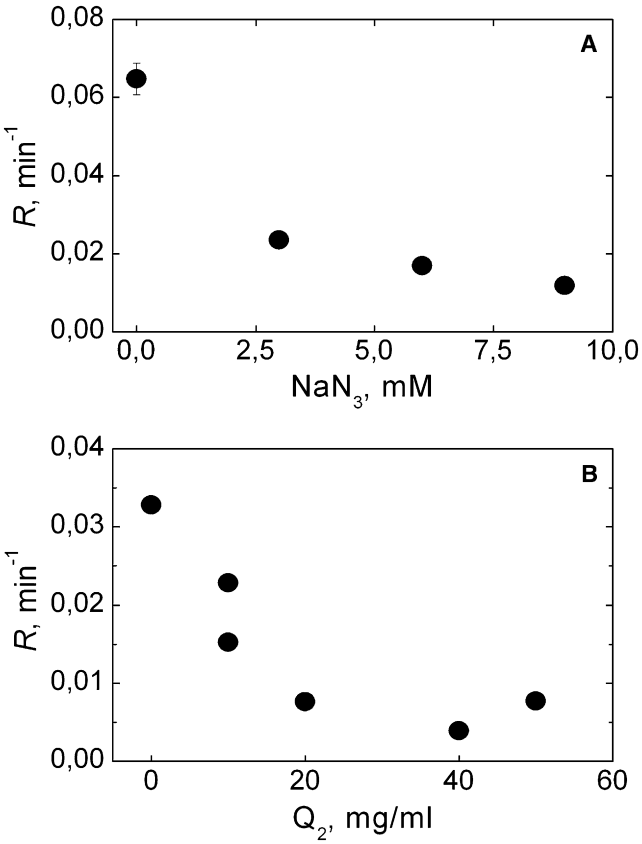

FIGURE 7 Effect of quenchers on the photoeffect. *R* (*trans* configuration) as a function of sodium azide concentration in the solution (*A*) and as a function of coenzyme Q2 concentration in the membrane (*B*). The concentration of AlPcS4 was either 50 μM (*A*) or 14 μM (*B*). All other conditions are similar to Fig. 3.

(24). We used an isoform with a short isoprenoid chain: coenzyme Q2. It appeared to very effectively protect the target. The antioxidant reduced the rate of the photodynamic reaction by about an order of magnitude (Fig. 7 *B*).

DISCUSSION

The photorelease of $^1O_2$ from the second leaflet resulted in the damage of target molecules bound to the second or the first leaflets. The dependence of the reaction rate on the sidedness of the target indicated that the $^1O_2$ concentrations ($[^1O_2]$) on the first and second membrane interfaces were different. This observation is surprising since the membrane thickness is small compared to the possible migration distances of $^1O_2$, both in water and in the membrane. There are two obvious explanations:

1. The membrane-impermeable reactive oxygen species contributed to the *cis* effect. The hypothesis contrasts with the observation that the limiting magnitude of the photoeffect V did not depend on the sidedness. This result suggested that the mechanism of photoreaction and the nature of the product were similar on both sides of the membrane. It is a type II photoreaction mediated by $^1O_2$. This conclusion is in line with the inhibition by sodium azide and coenzyme Q as well as with the observation that the photodynamic activity of $AlPcS_4$ is based on $^1O_2$ release (25,26).
2. P_{1O} is so small that the membrane represents a barrier to $^1O_2$ movement. As a result, $[^1O_2]$ at the first and second leaflets differ from each other.

Testing of hypothesis 2 requires evaluation of P_{1O}. By definition, P_{1O} is a proportionality coefficient linking transmembrane flow of $^1O_2$ and the difference in $^1O_2$ concentrations at both sides of the membrane:

$$J = P_{1O}\left([^1O_2]_2 - [^1O_2]_1\right), \tag{1}$$

where $[^1O_2]_1$ and $[^1O_2]_2$ are the corresponding $^1O_2$ concentrations at the first and second surfaces of the membrane, respectively. V and R also depend on $[^1O_2]_1$ and $[^1O_2]_2$. Consequently, P_{1O} can be assessed from V and R. For this purpose, we developed a mathematical model of the photodynamic reactions between phlorizin and $^1O_2$ that takes into account diffusion processes. The model allowed derivation of simple expressions for V and R (compare Appendix A):

$$R = -k_p[^1O_2]\left[1 - \frac{\mu_P\left(1 + 10^{pH-pK_A}\right)}{\mu_A\left(1 + 10^{pH-pK_P}\right)}\right],$$
$$V = 1 - \frac{k_d\mu_P\left(1 + 10^{pH-pK_A}\right)}{k_{pd}\mu_A\left(1 + 10^{pH-pK_P}\right)}, \tag{2}$$

where k_p is the reaction rate, μ_A and μ_P are the normal components of dipole moments of the target molecule and the product, pK_A and pK_P are the negative logarithms of their dissociation constants, and k_d and k_{pd} are the target and product desorption rate constants from the membrane into water solution. Eq. 2 describes the dependence of the photoeffect on pH (Fig. 6, *B* and *C*). It also reflects the dependence of R on light intensity (Fig. 5).

Consequently, the threefold decrease in R, which is observed when the configuration of the experiment is changed from *cis* to *trans*, indicates a threefold excess of $[^1O_2]_2$ over $[^1O_2]_1$. In the following, $[^1O_2]_1$ is derived from J assuming that all $^1O_2$ molecules appearing at the first interface escape into the aqueous solution and that all of them are subsequently quenched (compare Eq. 5B of Appendix B). The assumption is justified by the observation that the $^1O_2$ lifetime in the membrane exceeds the one in the aqueous solution 10-fold:

$$[^1O_2]_1 = \frac{J}{\sqrt{Dk_q}}, \tag{3}$$

where k_q and D are the decay rate in water and the diffusion coefficient of $^1O_2$, respectively. Insertion of Eq. 3 into Eq. 1 results in

$$[^1O_2]_1\sqrt{Dk_q} = P_{1O}\left([^1O_2]_2 - [^1O_2]_1\right). \tag{4}$$

According to Eq. 2, the ratio $[^1O_2]_2/[^1O_2]_1$ can be determined as

$$\frac{[^1O_2]_2}{[^1O_2]_1} = \frac{R_{cis}}{R_{trans}}. \tag{5}$$

Finally, P_{1O} is obtained as

$$P_{1O} = \frac{\sqrt{Dk_q}}{\frac{R_{cis}}{R_{trans}} - 1}. \tag{6}$$

From $R_{cis}/R_{trans} \approx 3$ (Fig. 5) follows that $P_{1O} \approx 2$ cm/s if it is assumed that k_q and D are equal to $3 \times 10^5\ s^{-1}$ (27,28) and $4.75 \times 10^{-5}\ cm^2\ s^{-1}$ (29), respectively.

In the presence of quenchers, P_{1O} decreases. For example, coenzyme Q augments R_{cis}/R_{trans} 10-fold, thereby decreasing P_{1O} to 0.3 cm/s. Consequently, P_{1O} has to be treated as an apparent permeability, which reflects the true membrane mobility of $^1O_2$ in the absence of quenchers. In that limiting case P_{1O} may be expected to be equal to P_O. Using pure model membranes which lacked unsaturated lipids and strict placement of target molecules only at the interface, we approached that limiting case as much as possible. However, P_O for model membranes has been determined by ESR to be equal to 210–230 cm/s (at 37°C–45°C) in the absence of cholesterol (2,4). Even if we assume that this value drops to 190 cm/s at room temperature for a fluid membrane, it is still two orders of magnitude larger than P_{1O}.

The reason for this discrepancy is not clear. ESR allows very precise measurement of both the concentration and the mobility of oxygen within the membrane. According to Overton's rule, these parameters are sufficient for calculating

membrane permeability. However, Overton's rule also predicts that

$$P_O \approx P_{NH3}(K_O/K_{NH3}) \approx P_{CO2}(K_O/K_{CO2}) \approx 10\text{cm s}^{-1} \quad (7)$$

where $K_O \sim 2$ (2,4), $K_{CO2} \sim 1.5$ (30), $K_{NH3} \sim 0.002$ (31), $P_{NH3} = 0.016$ cm/s (32), and $P_{CO2} = 3.2$ cm/s (33). Thus, Eq. 7 predicts an oxygen permeability that is much closer to P_{1O} than the permeability derived from ESR data. Assuming that O_2, NH_3, and CO_2 have comparable membrane diffusivities and that none of them belongs to those extremely rare exceptions to Overton's rule (31,34), Eq. 7 may give the best possible estimate of P_O since it is based on direct permeability measurements.

The difference between P_O and P_{1O} may be due to an underestimation of P_{1O} because we neglected $^1O_2$ diffusion into the membrane torus. As a consequence, its concentration within the lipid bilayer decreases. In turn, some of the target molecules are prevented from being damaged. The effect is limited to a 600-nm-wide band adjacent to the torus, as calculated from the $^1O_2$ lifetime of 35 μs. Since the membrane radius always exceeded 1.5 mm, the area with undamaged targets may be neglected.

Finally, surface diffusion of hydrophobic products away from the area of the lipid bilayer to the membrane torus may also lead to an underestimation of P_{1O}. This phenomenon is important only in *trans* configuration when $^1O_2$ has to cross the torus to reach the target. Since the torus has to expand beyond the bilayer center to approximately match the thickness of the Teflon septum (~30 μm), its thickness exceeds 600 nm in most of its parts. The torus is, thus, mainly impermeable to $^1O_2$. Consequently, a product concentration gradient is expected to appear at the lipid-water interface between the bilayer area and the torus region. This gradient gives rise to product diffusion out of the lipid bilayer area, which, in turn, decreases the absolute value of $\Delta\varphi_b$ and thus leads to an underestimation of R_{trans}. A similar effect is missing in *cis* configuration, as the photodynamic reaction occurs at the water-lipid interfaces of both the bilayer and the torus regions.

We therefore conclude that the value of 2 cm/s only represents the lower limit of P_{1O}. Nevertheless, it rules out the possibility that the membrane acts as a barrier to $^1O_2$ diffusion. CO_2 diffusion across the membrane occurs at roughly the same speed, and it is known that CO_2 transport is limited by diffusion through near-membrane stagnant water layers and not by diffusion through the membrane itself (33,35,36). Our result is in agreement with Overton's rule, which predicts that O_2 and CO_2 have roughly similar permeabilities. In the absence of $^1O_2$ quenchers, the apparent difference in the reaction rates on the two sides of the membrane is due to product diffusion away from the bilayer surface to the surface of adjacent lipids. In a biological system, differences in the reaction rates at the cytoplasmic and extracellular leaflets are also expected to exist, since intramembrane quenchers are unavoidably present.

APPENDIX A: MODEL OF THE PHOTODYNAMIC REACTION

The current model of the photodynamic reaction is a modified version of an already published model (9). As before, $^1O_2$ is released from membrane-bound $AlPcS_4$, and it is assumed that the target is oxidized without detailing the chemistry of the reaction. In contrast to the previous model, target and product are unable to cross the membrane. Consequently, *cis* and *trans* configurations can be distinguished where target and $^1O_2$ source are adsorbed to the same or to opposite leaflets, respectively. In the first case, $^1O_2$ reacts with phlorizin immediately; in the second case it reacts after diffusion through the membrane (Fig. 1). The mechanism of the reversible reaction is assumed to be identical in both cases. The changes of the membrane surface concentrations of phlorizin and of the product, A_m and P_m, respectively, are described by the following differential equations:

$$\frac{d}{dt}A_m = k_a A_w - k_d A_m - k_p[^1O_2]A_m + k_r P_m \quad (1A)$$

$$\frac{d}{dt}P_m = -k_{pd}P_m + k_p[^1O_2]A_m - k_r P_m, \quad (2A)$$

where k_{Pd} is the rate constant of product desorption. The rate constants of the forward and reverse reactions are denoted k_p and k_r, respectively. Phlorizin adsorption and desorption occurs with the rate constants k_a and k_d, respectively.

Before illumination (time $t = 0$), there is no product and A_m is in equilibrium with the aqueous phlorizin concentration (A_W):

$$P_m|_{t=0} = 0;\ A_m|_{t=0} = \frac{k_a}{k_d}A_W. \quad (3A)$$

The solution of Eqs. 1A–2A with the initial conditions (Eq. 3A) is a sum of two exponential functions. However, the initial rate and the steady-state product concentration can be determined without finding the exact solution. From Eq. 3A and Eqs. 1A–2A, we obtain for $t = 0$

$$\left.\frac{dA_m}{dt}\right|_{t=0} = -k_p[^1O_2]A_m \left.\frac{dP_m}{dt}\right|_{t=0} = k_p[^1O_2]A_m, \quad (4A)$$

and for $t \to \infty$,

$$P_m|_{t\to\infty} = \frac{k_a A_W k_p[^1O_2]}{k_{pd}k_p[^1O_2] + k_d k_r + k_{pd}k_d},$$

$$A_m|_{t\to\infty} = \frac{k_a A_W (k_r + k_{pd})}{k_{pd}k_p[^1O_2] + k_d k_r + k_{pd}k_d}. \quad (5A)$$

Equation 5A assumes that the volume of the bulk solution is so large that it serves as an infinite source of phlorizin and an ideal sink of the photoproduct, i.e., A_W does not change with time and the aqueous bulk concentration of the product is negligible.

As a result of the photodynamic reaction, A_m, and thus the contribution of the reactant to $\Delta\varphi_b$, decreases. A product P_m is accumulated, which also contributes to $\Delta\varphi_b$:

$$\Delta\varphi_{b,A} = \alpha A_m \quad (6A)$$

$$\Delta\varphi_{b,P} = \beta P_m. \quad (7A)$$

The total dipole potential is

$$\Delta\varphi_b = \Delta\varphi_{b,A} + \Delta\varphi_{b,p}.$$

From Eqs. 3A–4A and 6A–7A, we can determine the initial rate of normalized potential change:

$$R|_{t=0} = \left.\frac{\frac{d\phi}{dt}}{\Delta\phi}\right|_{t=0} = \left.\frac{\alpha\frac{dA_m}{dt} + \beta\frac{dP_m}{dt}}{\alpha A_m + \beta P_m}\right|_{t=0} = -k_p[^1O_2]\left(1-\frac{\beta}{\alpha}\right). \tag{8A}$$

R is proportional to the rate constant of the photodynamic reaction and, thus, to $[^1O_2]$. Equations 3A, 5A, and 6A–7A allow determination of the ratio of the steady-state dipole potential to the initial potential:

$$\frac{\Delta\phi|_{t\to\infty}}{\Delta\phi|_{t=0}} = \frac{\alpha k_d(k_r + k_{pd}) + \beta k_d k_p[^1O_2]}{\alpha\left(k_{pd}k_p[^1O_2] + k_d k_r + k_{pd}k_d\right)}. \tag{9A}$$

A parameter which is experimentally more convenient to assess is the relative amplitude of potential change V:

$$V = \frac{\Delta\phi|_{t\to\infty} - \Delta\phi|_{t=0}}{\Delta\phi|_{t=0}} = 1 - \frac{\alpha k_d(k_r + k_{pd}) + \beta k_d k_p[^1O_2]}{\alpha\left(k_{pd}k_p[^1O_2] + k_d k_r + k_{pd}k_d\right)}. \tag{10A}$$

V increases with the reaction rate until an upper limit is reached, which can be predicted assuming that $[^1O_2]$ reaches infinity:

$$V|_{k_p\to\infty} = 1 - \frac{k_d\beta}{k_{pd}\alpha}. \tag{11A}$$

The unknown parameters α and β can be determined from the pH dependence of $\Delta\varphi_b$. $\Delta\varphi_b$ is generated by membrane adsorption of protonated phloretin or phlorizin molecules (13,14,37). It is calculated as if the planar capacitor would be charged:

$$\Delta\phi_{b,A} = \frac{\mu_A}{\varepsilon\varepsilon_0}[AH]_m, \tag{12A}$$

where μ_A is the component of the phlorizin's dipole moment normal to the membrane surface, ε is the dielectric permittivity of the medium, ε_0 is the electric constant, and $[AH]_m$ is the surface concentration of the adsorbed neutral phlorizin molecules. Assuming that the photodynamic damage of phlorizin is so slow that proton release by phlorizin is close to equilibrium, $[AH]_m$ is calculated as

$$[AH]_m = \frac{A_m}{1 + K_A/H}, \tag{13A}$$

where K_A and H are the dissociation constant and the proton concentration, respectively. Eqs. 6A, 12A, and 13A allow determination of α:

$$\alpha = \frac{\mu_A}{\varepsilon\varepsilon_0}\frac{H}{H + K_A}. \tag{14A}$$

Assuming that the properties of the reactant and of the product are not fundamentally different, we arrive at a similar expression for β:

$$\beta = \frac{\mu_P}{\varepsilon\varepsilon_0}\frac{H}{H + K_P}, \tag{15A}$$

where μ_P and K_P are the normal component of the product's dipole moment and the dissociation constant, respectively. Using Eqs. 14A and 15A, Eqs. 8A and 11A can be rewritten (compare Eq. 2):

$$R = -k_p[^1O_2]\left[1 - \frac{\mu_P(H + K_A)}{\mu_A(H + K_P)}\right],$$
$$V = 1 - \frac{k_d\mu_P(H + K_A)}{k_{pd}\mu_A(H + K_P)}.$$

APPENDIX B: INTERFACIAL $^1O_2$ CONCENTRATION

Calculation of membrane permeability, P_{1O}, requires knowledge of the steady-state concentration $[^1O_2]$ at both membrane leaflets. The differential equation for the coupled diffusion and reaction processes is simplified by the assumption that most of the $^1O_2$ molecules are quenched in water and only a negligible amount is consumed by the reaction with phlorizin. Consequently, in the steady state $[^1O_2]$ at the first side is given by

$$0 = -k_q[^1O_2](x) + D\frac{d^2[^1O_2](x)}{dx^2}, \tag{1B}$$

where x is the distance from the membrane-water interface. Two boundary conditions apply:

1. The $^1O_2$ transmembrane flow J is equal to the $^1O_2$ flow through the aqueous layers in the immediate vicinity of the first membrane-water interface. It is derived according to Fick's law of diffusion:(2B)

$$J = -D\left.\frac{d[^1O_2](x)}{dx}\right|_{x=0}. \tag{2B}$$

2. $^1O_2$ has a limited lifetime in solution, i.e., all $^1O_2$ molecules are quenched at some distance l to the membrane:(3B)

$$[^1O_2](x)|_{x=l} = 0. \tag{3B}$$

Integration of Eq. 1B results in

$$[^1O_2](x) = [^1O_2]_1\exp\left(-x\sqrt{\frac{k_q}{D}}\right). \tag{4B}$$

Eq. 4B can easily be solved for $x = 0$:

$$[^1O_2](x)|_{x=0} = [^1O_2]_1 = \frac{J}{\sqrt{Dk_q}}. \tag{5B}$$

SUPPLEMENTARY MATERIAL

One figure is available at http://www.biophysj.org/biophysj/supplemental/S0006-3495(08)00021-0.

We thank Quentina Beatty and Alexander Lents for editorial help.

The project was supported by the Deutsche Forschungsgemeinschaft (Po 533/4), by the president of the Russian Federation (in support of Leading Scientific Schools No. 4181.2008.4), and by the presidium of the Russian Academy of Sciences (grant "Molecular and Cell Biology").

REFERENCES

1. Levy, J. G. 1994. Photosensitizers in photodynamic therapy. *Semin. Oncol.* 21:4–10.
2. Subczynski, W. K., J. S. Hyde, and A. Kusumi. 1989. Oxygen permeability of phosphatidylcholine–cholesterol membranes. *Proc. Natl. Acad. Sci. USA*. 86:4474–4478.

3. Subczynski, W. K., J. S. Hyde, and A. Kusumi. 1991. Effect of alkyl chain unsaturation and cholesterol intercalation on oxygen-transport in membranes—a pulse ESR spin labeling study. *Biochemistry*. 30:8578–8590.
4. Dzikovski, B. G., V. A. Livshits, and D. Marsh. 2003. Oxygen permeation profile in lipid membranes: comparison with transmembrane polarity profile. *Biophys. J.* 85:1005–1012.
5. Subczynski, W. K., L. E. Hopwood, and J. S. Hyde. 1992. Is the mammalian-cell plasma-membrane a barrier to oxygen transport? J. Gen. Physiol. 100:69–87.
6. Ehrenberg, B., J. L. Anderson, and C. S. Foote. 1998. Kinetics and yield of singlet oxygen photosensitized by hypericin in organic and biological media. *Photochem. Photobiol.* 68:135–140.
7. Dearden, S. J. 1986. Kinetics of $O_2(^1\text{-}\Delta_g)$ photo-oxidation reactions in egg-yolk lecithin vesicles. *J. Chem. Soc. Faraday Trans. I.* 82:1627–1635.
8. Hoebeke, M., J. Piette, and A. Vandevorst. 1991. Photosensitized production of singlet oxygen by merocyanine-540 bound to liposomes. *J. Photochem. Photobiol. B.* 9:281–294.
9. Sokolov, V. S., I. N. Stozhkova, M. Block, and P. Pohl. 2000. Membrane photopotential generation by interfacial differences in the turnover of a photodynamic reaction. *Biophys. J.* 79:2121–2131.
10. Rezk, B. M., G. R. Haenen, W. J. van der Vijgh, and A. Bast. 2002. The antioxidant activity of phloretin: the disclosure of a new antioxidant pharmacophore in flavonoids. *Biochem. Biophys. Res. Commun.* 295:9–13.
11. Andersen, O. S., A. Finkelstein, and I. Katz. 1976. Effect of phloretin on the permeability of thin lipid membranes. *J. Gen. Physiol.* 67:749–771.
12. Melnik, E., R. Latorre, J. E. Hall, and D. C. Tosteson. 1977. Phloretin-induced changes in ion transport across lipid bilayer membranes. *J. Gen. Physiol.* 69:243–257.
13. Sokolov, V. S., V. V. Cherny, and V. S. Markin. 1984. Measurements by inner field compensation method of the potential induced by phloretin and phlorezin adsorption on BLM. *Biofizika.* 29:424–429.
14. Pohl, P., T. I. Rokitskaya, E. E. Pohl, and S. M. Saparov. 1997. Permeation of phloretin across bilayer lipid membranes monitored by dipole potential and microelectrode measurements. *Biochim. Biophys. Acta.* 1323:163–172.
15. Mueller, P., D. O. Rudin, H. T. Tien, and W. C. Wescott. 1963. Methods for the formation of single bimolecular lipid membranes in aqueous solution. *J. Phys. Chem.* 67:534–535.
16. Rokitskaya, T. I., Y. N. Antonenko, and E. A. Kotova. 1993. The interaction of phthalocyanine with planar lipid bilayers—photodynamic inactivation of gramicidin channels. *FEBS Lett.* 329:332–335.
17. Stozhkova, I. N., V. V. Cherny, V. S. Sokolov, and Y. A. Ermakov. 1997. Adsorption of haematoporphyrins on the planar bilayer membrane. *Membr. Cell Biol.* 11:381–399.
18. Rokitskaya, T. I., M. Block, Y. N. Antonenko, E. A. Kotova, and P. Pohl. 2000. Photosensitizer binding to lipid bilayers as a precondition for the photoinactivation of membrane channels. *Biophys. J.* 78:2572–2580.
19. Sokolov, V. S., and V. G. Kuzmin. 1980. Study of surface potential difference in bilayer membranes according to the second harmonic response of capacitance current. *Biofizika.* 25:170–172.
20. Ermakov, Y. A., and V. S. Sokolov. 2003. Boundary potentials of bilayer lipid membranes: methods and interpretations. *In* Planar Lipid Layers (BLMs) and Their Applications. H. T. Tien and A. Ottova-Leitmannova, editors. Elsevier, Amsterdam, 109–141.
21. Sokolov, V. S., and V. M. Mirsky. 2004. Electrostatic potentials of bilayer lipid membranes: basic research and analytical applications. *In* Ultrathin Electrochemical Chemo- and Biosensors: Technology and Performance. V. M. Mirsky, editor. Springer, Berlin, Heidelberg, Germany, 255–291.
22. Alvarez, O., and R. Latorre. 1978. Voltage-dependent capacitance in lipid bilayers made from monolayers. *Biophys. J.* 21:1–17.
23. Varnes, M. E., M. T. Bayne, H. J. Menegay, and S. W. Tuttle. 1993. Effect of the potassium/proton ionophore nigericin on response of A549 cells to photodynamic therapy and tert-butylhydroperoxide. *Free Radic. Biol. Med.* 15:395–405.
24. Cabrini, L., P. Pasquali, B. Tadolini, A. M. Sechi, and L. Landi. 1986. Antioxidant behaviour of ubiquinone and β-carotene incorporated in model membranes. *Free Radic. Res. Commun.* 2:85–92.
25. Bachowski, G. J., E. Ben-Hur, and A. W. Girotti. 1991. Phthalocyanine-sensitized lipid peroxidation in cell membranes: use of cholesterol and azide as probes of primary photochemistry. *J. Photochem. Photobiol. B.* 9:307–321.
26. Niedre, M., M. S. Patterson, and B. C. Wilson. 2002. Direct near-infrared luminescence detection of singlet oxygen generated by photodynamic therapy in cells in vitro and tissues in vivo. *Photochem. Photobiol.* 75:382–391.
27. Rodgers, M. A. J., and P. T. Snowden. 1982. Lifetime of singlet oxygen in liquid water as determined by time resolved infrared luminescence measurements. *J. Am. Chem. Soc.* 104:5541–5543.
28. Krasnovsky, A. A. Jr. 1998. Singlet molecular oxygen in photobiochemical systems: IR phosphorescence studies. *Membr. Cell Biol.* 12:665–690.
29. Fischkoff, S., and J. M. Vanderkooi. 1975. Oxygen diffusion in biological and artificial membranes determined by fluorochrome pyrene. *J. Gen. Physiol.* 65:663–676.
30. Simon, S. A., and J. Gutknecht. 1980. Solubility of carbon dioxide in lipid bilayer membranes and organic solvents. *Biochim. Biophys. Acta.* 596:352–358.
31. Walter, A., and J. Gutknecht. 1986. Permeabilities of small neonelectrolytes through lipid bilayer membranes. *J. Membr. Biol.* 90:207–217.
32. Antonenko, Y. N., P. Pohl, and G. A. Denisov. 1997. Permeation of ammonia across bilayer lipid membranes studied by ammonium ion selective microelectrodes. *Biophys. J.* 72:2187–2195.
33. Missner, A., P. Kugler, S. M. Saparov, K. Sommer, J. C. Matthai, et al. 2008. Carbon dioxide transport through membranes. *J. Biol. Chem.* 283:25340–25347.
34. Saparov, S. M., Y. N. Antonenko, and P. Pohl. 2006. A new model of weak acid permeation through membranes revisited: does Overton still rule? Biophys. J. 90:L86–L88.
35. Gutknecht, J., M. A. Bisson, and D. C. Tosteson. 1977. Diffusion of carbon dioxide through lipid bilayer membranes. Effects of carbonic anhydrase, bicarbonate and ustirred layers. *J. Gen. Physiol.* 69:779–794.
36. Yang, B. X., N. Fukuda, A. van Hoek, M. A. Matthay, T. H. Ma, et al. 2000. Carbon dioxide permeability of aquaporin-1 measured in erythrocytes and lung of aquaporin-1 null mice and in reconstituted proteoliposomes. *J. Biol. Chem.* 275:2686–2692.
37. DeLevie, R., S. Rangarajan, P. Seelig, and O. S. Andersen. 1979. On the adsorption of phloretin onto a black lipid membrane. *Biophys. J.* 25:295–300.